WILEY-VCH

Janus Graphene: Scalable Self-assembly and Solution-Phase Orthogonal Functionalization

*Intak Jeon, Martin D. Peeks, Suchol Savagatrup, Lukas Zeininger, Sehoon Chang, Gawain Thomas, Wei Wang and Timothy M. Swager**

Dr. Intak Jeon, Dr. Martin D. Peeks, Dr. Suchol Savagatrup, and Prof. Timothy M. Swager*
Department of Chemistry, Institute for Soldier Nanotechnologies
Massachusetts Institute of Technology
Cambridge, Massachusetts 02139, USA
E-mail: tswager@mit.edu

Dr. Sehoon Chang, Gawain Thomas, and Dr. Wei Wang
Aramco Services Company
Aramco Research Center-Boston
Cambridge, Massachusetts 02139, USA

Dr. Lukas Zeininger
Department of Chemistry
Massachusetts Institute of Technology
Cambridge, Massachusetts 02139, USA

Keywords: Janus, graphene, interfacial trapping, self-assembly, interfacial arrangement

Orthogonal functionalization of two-dimensional (2-D) materials by selective assembly at interfaces provides opportunities to create new materials with transformative properties. Challenges remain in realizing controllable, scalable surface-selective and orthogonal functionalization. Herein, we report dynamic covalent assembly that directs the functionalization of graphene surfaces at liquid−liquid interfaces. This process allows for facile addition and segregation of chemical functionalities to impart Janus characteristics to graphenes. Specifically, the dynamic covalent functionalization is accomplished via Meisenheimer complexes produced by reactions of primary amines with pendant dinitroaromatics attached to graphenes. Janus graphenes are demonstrated to be powerful surfactants that organize at water/organic, water/fluorocarbon, and organic/fluorocarbon liquid interfaces. This approach provides general access to the creation of diverse surfactant materials and promising building blocks for 2-D materials.

Multi-functional materials that leverage anisotropic intermolecular interactions find many useful applications in biomedical, sensing, and morphological templating.[1-9] For example, polymers with two asymmetric functional groups displaying preferential orientations at the air–water interface allow for precise presentation of chemical features, depending on the affinity of functional groups.[10] We have targeted disc-shaped Janus objects that display remarkable stabilization at oil−water interfaces.[11] In this context, graphenes have the potential for asymmetric functionalization on its surfaces. However, orthogonal functionalization of the two basal planes of graphene sheets remains a challenge and two-dimensional (2-D) Janus graphene (**JG**) architectures are rare.[12-19] Herein we report a highly controllable, scalable and versatile strategy for the fabrication of 2-D Janus graphene nanosheets via dynamic covalent functionalization of a functionalized graphene precursor at the liquid−liquid interface. We demonstrate the utility of 2-D **JG** for oil recovery as Pickering emulsifiers, potential membrane precursors, and for the stabilization of complex interfaces.

The interfacial trapping and lateral self-assembly of 3,5-dinitrophenyl functionalized graphenes (**FGs**) at the ethyl acetate−water interface affords the opportunity to explore differential functionalization at interfaces to create 2-D **JGs** (**Figure 1a**). The **FG** has 3,5-dinitrophenyl groups on the π-conjugated surfaces of both basal planes that reduce intersheet interactions and stacking, in contrast to the strong π−π attractions between pristine graphene sheets (**Figure S1**).[20] This allows individual sheets of **FGs** in 2-D assemblies to simultaneously interact with two different liquids at an interface (**Figure 1a**). Once organized at an interface, the anisotropic disc-like **FGs** (width/thickness ratio ~ 40) experience attractive capillary interactions, leading to laterally edge-packed structures (**Figure 1b**).[20, 21] This organization allows for the controllable functionalization with linear hydrocarbon, fluorocarbon, and/or water-soluble-ethylene oxide chains of the two separate **FG** surfaces to produce **JGs** (**Figure 1c**). The functionalization is accomplished by amine addition to the electron deficient 3,5-dinitrophenyl groups on the graphene basal planes. The resulting connections involve reversible covalent bonds through Meisenheimer complexes formation, which occurs at liquid−liquid interfaces. We confirm the asymmetric nature and functionalization of the **JGs** by interfacial studies and spectroscopic methods.

Figure 2 and **Figure S2** illustrate the two-dimensional assembly of **FG** at the liquid−liquid interface for various solvent pairs. During the agitation of liquids with **FGs**, **FGs** are trapped with the kinetic adsorption of air at the water−organic interface (**Figure 2a**). This mechanism depends on the ability of the **FG** and air to competitively adsorb at the interface, which is related to the liquid−air interfacial tension (**Figure 2b**). Trapped air is relatively energetically unfavorable and **FG** decreases the free energy of the system, resulting in its assembly at the liquid−liquid interface. The trapping efficiency of **FGs** depends on the energy contribution of air at the interface of immiscible liquids, as can be briefly expressed by:[22-24]

$$\textbf{FG}\ \text{trapping efficiency} \propto \gamma_{w-a} - \gamma_{s-a} - \gamma_{w-s}$$

where γ_{w-a}, γ_{s-a}, and γ_{w-s} are interfacial tension of water−air, solvent−air, and water−solvent, respectively.[25-27] Although the interfacial tension of **FG-**liquid is excluded, air dominantly contributes to the interfacial trapping efficiency. The water−ethyl acetate system shows the most unfavorable interfacial adsorption of air and thereby affords a high interfacial area for the assembly of materials (**Figure 2b**). As a result, **FG** is most effectively trapped at the interface of the immiscible combination of ethyl acetate and water (**Movie 1**). The **FG** assembly decreases the ethyl acetate−water interfacial tension to a value of 6.33 mN m^{-1} at 21 °C, measured by the Du Noüy ring method. According to Binks' analysis, the free energy of detachment (ΔG_{dw}) of a disc-like **FG** (width/thickness ratio ~ 40) into water is expressed by:[28-31]

$$\Delta G_{dw} = \gamma_{w-s}\pi b^2(1-cos\theta)^2 \times (aspect\ ratio\ dependency)$$

where θ is the three-phase contact angle with the disc-like particle, and b is the length of the disc-like particle in its minor (short) semi-axis. The **FG** is 2.4 nm-thick and the disc-like **FG** is expected to be strongly trapped at the interface ($\Delta G_{dw} \gg k_B T$). The assembly of **FG** has a face-on structure that orients with each side-facing opposite liquid interfaces (**Figure 1b**). Alternatively, if air is competitive for the interface as in Case 2, kinetically trapped air reduces the efficiency of the interfacial trapping of **FGs** at the interface. The partitioning of carbon materials in mixed solvents depends on their solubility or dispersibility (**Figure 2d**). Graphene, reduced graphene oxide (**rGO**), and unfunctionalized carbon nanotubes (**CNT**) all lack strong interactions with solvents and therefore can also be trapped at an ethyl acetate−water interface. However, these carbon nanomaterials randomly aggregate as a result of their strong π−π interactions. Other materials that are strongly dissolved and dispersed in solvents. For example, water-soluble graphene oxide (**GO**) with dense oxygenated groups, cannot be organized at

these interfaces. Thus, **FG** with greatly reduced sheet-to-sheet interactions organizes into equilibrium structures at interfaces and can be reactively converted into a Janus structure.

Hansen solubility parameters (**Table S1**) provide an intuitive tool for the selection of compatible solvents for interfacial trapping of carbon nanotube and graphene dispersions.[32, 33] We successfully selected solvents that concentrate **FG** at their interfaces with water.[34] Appropriate solvents for interfacial trapping have $14.5 < \delta_D < 15.8$ MPa$^{0.5}$, $2.9 < \delta_P < 8.4$ MPa$^{0.5}$ and $3.5 < \delta_H < 10.2$ MPa$^{0.5}$, where δ_D, δ_P, and δ_H are the dispersive, polar, and hydrogen bonding solubility parameters (**Figure 2d**). As expected, the ethyl acetate−water combination is the most effective system. Our findings show that **FG** assembles into a well-defined film at the liquid−liquid interface when three requirements are met: (i) Two liquids must be largely immiscible to generate an interface. (ii) The solvents must only weakly solvate the graphenes. **FG**, **rGOs**, **CNTs**, and **graphenes** occupy the interface of water and ethyl acetate, whereas fully solvated **GOs** have too great an affinity for the bulk water. (iii) The solvents need to have lower interfacial tension with water than with air. For example, solvents containing hydrogen bonding acetate ester (CH_3CO_2−R) and ether (R−O−R′) groups cause **FG** to assemble at the organic−water interface. To transport the **FG** from the bulk phase to the liquid−liquid interface requires the external mechanical force that breaks the two immiscible liquid phases into emulsion droplets with **FG** separating the two liquids (**Figure S3a**). During agitation, the **FG** quickly moves to the water−ethyl acetate interface by Rayleigh-Bénard convection (**Figure S3a**).[35] Finally, at equilibrium, the **FG** is preferentially adsorbed at the water−ethyl acetate interface. At a transient stage, the **FG** and air bubbles both encapsulate water at the interface (**Figure S3b and Movie 2**). Then the **FG** assembles, the air bubbles collapse, and the encapsulated water joins the bulk water. The strongly interfacially trapped **FG** moves with the interface while the weakly trapped air layer remains at the initial position. In case of a low-density assembly of **FG**, the addition of a rhodamine B dye induces a gradient of the interfacial tension at the interface that rearranges the assembly of **FG** and air bubbles (**Figure S3c and Movie 3**). The results are consistent with the interfacial trapping of **FG** in a water−ethyl acetate−kinetically trapped air system. When the concentration of **FG** is high enough, it fully saturates the interface and reaches the critical interfacial concentration for stable Pickering emulsion formation (**Figure S3d**).

Once the **FG** assemblies are trapped at an interface, they can then be reacted to produce Meisenheimer complexes with *n*-octylamine (**H**) or 1*H*,1*H*,2*H*,2*H*-perfluorooctylamine (**F**) in ethyl acetate, and 4,7,10-trioxa-1,13-tridecanediamine (**W**) chains in water (**Figure 3a** and **Figure S4**). After the **H** or **F** chains in ethyl acetate phase add to the surface, they tightly anchor **FG** at the interface (**Figure 3b** and **Figure S5**). Subsequently, water-soluble linear **W** chains are added into the water phase so that the **FG** surface facing the water can also be functionalized through Meisenheimer complexes formation (**Figure 3c**). As the glass of the vial is hydrophilic, driven by Marangoni force, the hydrophilic surface of the **JG** climbs the wall spreading the hydrophobic surface of the mixed ethyl acetate-hexane solution (**Figure 3d** and **Movie 4**). Most importantly, nearly all **JGs** continued to remain at the interface, indicating a strong adsorption at the interface. Notably, the well-defined and orthogonally functionalized **JGs** are efficiently trapped and their basal planes are self-assembled at the interface. The persistent structure at the interface enables sequential chemical modifications with the graphene surfaces facing the water being functionalized with ethylene oxide groups and the surfaces facing the organic phase being functionalized separately (**Figure 3e** and **Figure 3f**). **JG-3** can be produced by a similar method as in **Figure 3g**. The **FG** starting material has an average thickness of 2.4 ± 0.2 nm with an mean lateral area of 0.012 μm^2 as determined by transmission electron microscopy (TEM) and atomic force microscope (AFM) measurements (**Figure S6** and **Figure S7**). The average AFM heights of **FG-H** and **JG-1** are found to be 3.4 ± 0.4 nm and 4.7 ± 0.4 nm, respectively. These thickness measurements show that the stepwise surface-selective orthogonal functionalization on graphenes is easily achieved through our method. As a further support for the successful formation of **JGs** or single surface grafting through

interfacial trapping and Meisenheimer complexes, we performed diffusion-ordered NMR spectroscopy (NMR ^{1}H DOSY), attenuated total reflectance-Fourier transform infrared spectroscopy (ATR-FTIR), and X-ray photoelectron spectroscopy (XPS) analysis (**Figure S8** and **Figure S9**). From NMR ^{1}H DOSY, we observed the **H** and **W** groups to be attached to the slowly diffusing graphenes. The asymmetrical functionalities on the two surfaces of the nanometer thick **JGs** create powerful new surfactant 2-D materials for interfacial chemistry and biology.

The Janus graphenes with two chemically different compartments show unique activities at liquid interfaces. First, **JG-1** climbs the walls of a glass vial as a result of a high-energy interface created by a thin layer of water on the hydrophilic glass in contact with the hexane to minimizing the interfacial energy (**Figure 4a** and **Movie 4**). We can induce non-spherical emulsions with kinetically jammed **JG-1s** by the restriction of equilibrium shapes (**Figure 4a**).[36] When the total area of **JG-1** surfactants oversaturates the area of the liquid interface ($\sum A_{JG-1} > A_{Interface}$), jammed assembly of **JG-1** arrests the non-equilibrium shapes of hexane in water. **JG-1** with orthogonally distinguishable hydrophobic and hydrophilic surfaces follows the rules for the interactions of the menisci: similar menisci attract and dissimilar menisci repel.[37] Thermodynamics drives **JG-1** to assemble into a continuous structure, and such processes have potential utility in the production of barrier or membrane structures. Water droplets added through the non-aqueous phase slide freely on the hydrophobic assembled graphene surface and are supported by this dense **JG-1** assembly (**Figure 4b**). The graphene layer prevents the water droplet from coalescing with the bottom water reservoir, confirming that the added water is segregated by a mechanically robust hydrophobic surface. Janus graphene can also be used as a chemical-enhanced oil recovery (CEOR) reagent. To demonstrate usage of **JG-1** in CEOR applications, we used a microfluidic-based reservoir model to understand oil-water-rock phase interactions and visualize the fluid transport processes in micropores (**Figure S10**).[38] **Figure 4c** shows the oil distribution after flooding the micropores using water with **JG-1** (91 μg mL^{-1}). In the presence of **JG-1**, a 14% improvement in oil recovery was observed compared to pure water (**Figure 4c** and **Figure S11**).[13] The result illustrates the opportunity for functionalized Janus 2-D surfactants to be utilized for extraction of organics from water and oil recovery applications.

We further observe surfactant-like interfacial phenomena of the **JG-2** layer when its surface density increases (**Figure 4d**). At high interfacial density of **JG-2**, the layer becomes unstable and then folds to form a bilayer, or 3-D aggregates. **Figure 4d** and **Movie 5** show bi-layer formation: folding, growth and collapsing. It is similar to the way that micelles or lipids form in a bulk phase above the critical micelle concentration.[39] **Figure 4e** and **Movie 6** illustrate the rearrangement for **JG-3** that is trapped at the *1,2*-dichlorobenzene (*1,2*-DCB)/ethyl nonafluorobutyl ether (F-ether) interface. To validate whether **JG-3** behaves as a surfactant at the interface of hydrocarbon and fluorocarbon liquids, we used complex liquids that can convert into Janus configurations (**Figure S12**).[40] In the initial stage at 35 °C, **JG-3** is dispersed in the single phase of *1,2*-DCB/F-ether. During cooling below the upper consolute temperature (*T*c), phase separation of the *1,2*-DCB and F-ether occurs within the dispersed water droplets. The **JG-3** then localizes at the *1,2*-DCB/F-ether interface in the Janus droplet configuration (**Figure S13**), and these droplets show a lower *T*c than those without **JG-3**. These effects demonstrate the affinity of **JG-3** to both the hydrocarbon and fluorocarbon phases.

Conclusion

In summary, we have reported a method for synthesis of various **JGs** with different functionalities that is general, scalable, and provides new possibilities in interfacial chemistry. Fully occupied and trapped graphenes at immiscible interfaces of water and ethyl acetate enable each surface

to react with distinct chemical functions through Meisenheimer complex formation. In principle, various functional pairs can be covalently bonded onto each surface of graphene to create a wide diversity of **JGs**. When co-grafting different chemical functions on each side of graphene, each surface faces different liquid environments and the activity of **JGs** modifies the interface of liquids. In principle, this synthetic strategy towards **JGs** can be extended to other 2-D solid materials: **graphenes**, **FGs**, **rGOs**, functionalized **GOs**, **CNTs**, MoS_2, and 2-D metal–organic frameworks. 2-D tailored **JGs** enable functional hierarchical structures of interest to molecular biology and medicinal chemistry.

Supporting Information

Supporting Information is available from the Wiley Online Library or from the author.

Acknowledgements

I.J. and T.M.S. developed the concept for the research. I.J. designed the synthesis method for Janus graphenes, performed measurements and analyzed the data in the paper. I.J., M.D.P., S.S., and L.Z. conducted experiments involving emulsion fabrication, imaging and NMR studies. S.C., G.T., and W.W., conducted oil recovery test. I.J. and T.M.S. wrote, and all authors commented on, the manuscript. We thank Dr. M. He for the synthesis of 3,5-dinitrobenzenediazonium salts, G. Park at MIT bio-instrumentation lab (Prof. I. Hunter) for high speed camera measurements, and Dr W. W. Massefski for helpful discussions. M.D.P. thanks the English-Speaking Union for a Lindemann Trust Fellowship. S.S. was supported by an F32 Ruth L. Kirschstein National Research Service Award. L.Z. acknowledges support from the German Research Foundation (DFG, Grant No. ZE1121/1-1). We also thank the Institute for Soldier Nanotechnologies at MIT for use of equipment.

Received: ((will be filled in by the editorial staff))
Revised: ((will be filled in by the editorial staff))
Published online: ((will be filled in by the editorial staff))

References

[1] I. Bita, J. K. W. Yang, Y. S. Jung, C. A. Ross, E. L. Thomas, K. K. Berggren, *Science* **2008**, *321,* 939.
[2] E. Kopperger, J. List, S. Madhira, F. Rothfischer, D. C. Lamb, F. C. Simmel, *Science* **2018**, *359,* 296.
[3] H. Qiu, Z. M. Hudson, M. A. Winnik, I. Manners, *Science* **2015**, *347,* 1329.
[4] L. L. Ong, N. Hanikel, O. K. Yaghi, C. Grun, M. T. Strauss, P. Bron, J. Lai-Kee-Him, F. Schueder, B. Wang, P. F. Wang, J. Y. Kishi, C. Myhrvold, A. Zhu, R. Jungmann, G. Bellot, Y. G. Ke, P. Yin, *Nature* **2017**, *552,* 72.
[5] K. H. Roh, D. C. Martin, J. Lahann, *Nat. Mater.* **2005**, *4,* 759.
[6] X. M. Mao, Q. Chen, S. Granick, *Nat. Mater.* **2013**, *12,* 217.
[7] Y. F. Wang, Y. Wang, D. R. Breed, V. N. Manoharan, L. Feng, A. D. Hollingsworth, M. Weck, D. J. Pine, *Nature* **2012**, *491,* 51.
[8] S. Sacanna, M. Korpics, K. Rodriguez, L. Colon-Melendez, S. H. Kim, D. J. Pine, G. R. Yi, *Nat. Commun.* **2013**, *4,* 1688
[9] G. Singh, H. Chan, A. Baskin, E. Gelman, N. Repnin, P. Kral, R. Klajn, *Science* **2014**, *345,* 1149.
[10] J. Kim, T. M. Swager, *Nature* **2001**, *411,* 1030.
[11] Y. Nonomura, S. Komura, K. Tsujii, *Langmuir* **2004**, *20,* 11821.
[12] L. M. Zhang, J. W. Yu, M. M. Yang, Q. Xie, H. L. Peng, Z. F. Liu, *Nat. Commun.* **2013**, *4,* 1443.
[13] D. Luo, F. Wang, J. Y. Zhu, F. Cao, Y. Liu, X. G. Li, R. C. Willson, Z. Z. Yang, C. W. Chu, Z. F. Ren, *Proc. Natl. Acad. Sci. USA* **2016**, *113,* 7711.

[14] D. S. Yu, E. Nagelli, R. Naik, L. M. Dai, *Angew. Chem. Int. Edit.* **2011**, *50,* 6575.
[15] B. T. McGrail, J. D. Mangadlao, B. J. Rodier, J. Swisher, R. Advincula, E. Pentzer, *Chem. Commun.* **2016**, *52,* 288.
[16] Y. F. Yang, L. Zhang, X. T. Ji, L. X. Zhang, H. F. Wang, H. Y. Zhao, *Macromol. Rapid Comm.* **2016**, *37,* 1520.
[17] H. Wu, W. Y. Yi, Z. Chen, H. T. Wang, Q. G. Du, *Carbon* **2015**, *93,* 473.
[18] A. de Leon, B. J. Rodier, Q. M. Luo, C. M. Hemmingsen, P. R. Wei, K. Abbasi, R. Advincula, E. B. Pentzer, *ACS Nano* **2017**, *11,* 7485.
[19] A. Holm, J. Park, E. D. Goodman, J. M. Zhang, R. Sinclair, M. Cargnello, C. W. Frank, *Chem. Mater.* **2018**, *30,* 2084.
[20] I. Jeon, B. Yoon, M. He, T. M. Swager, *Adv. Mater.* **2018**, *30,* 1704538.
[21] P. J. Yunker, T. Still, M. A. Lohr, A. G. Yodh, *Nature* **2011**, *476,* 308.
[22] S. Sacanna, W. K. Kegel, A. P. Philipse, *Phys. Rev. Lett.* **2007**, *98,* 158301.
[23] E. Vignati, R. Piazza, T. P. Lockhart, *Langmuir* **2003**, *19,* 6650.
[24] R. McGorty, J. Fung, D. Kaz, V. N. Manoharan, *Mater. Today* **2010**, *13,* 34.
[25] J. J. Jasper, *Journal of physical and chemical reference data* **1972**, *1,* 841.
[26] A. H. Demond, A. S. Lindner, *Environ. Sci. Technol.* **1993**, *27,* 2318.
[27] Y. Lin, H. Skaff, T. Emrick, A. D. Dinsmore, T. P. Russell, *Science* **2003**, *299,* 226.
[28] B. P. Binks, T. S. Horozov, *Colloidal particles at liquid interfaces*, Cambridge University Press, Cambridge 2006.
[29] K. S. Kim, Y. Zhao, H. Jang, S. Y. Lee, J. M. Kim, K. S. Kim, J. H. Ahn, P. Kim, J. Y. Choi, B. H. Hong, *Nature* **2009**, *457,* 706.
[30] X. L. Li, G. Y. Zhang, X. D. Bai, X. M. Sun, X. R. Wang, E. Wang, H. J. Dai, *Nat. Nanotechnol.* **2008**, *3,* 538.
[31] J. Kim, L. J. Cote, F. Kim, W. Yuan, K. R. Shull, J. X. Huang, *J. Am. Chem. Soc.* **2010**, *132,* 8180.
[32] C. M. Hansen, *Hansen solubility parameters : a user's handbook*, CRC Press, Boca Raton 2007.
[33] Y. Hernandez, M. Lotya, D. Rickard, S. D. Bergin, J. N. Coleman, *Langmuir* **2010**, *26,* 3208.
[34] J. N. Coleman, *Acc. Chem. Res.* **2013**, *46,* 14.
[35] J. Shim, J. M. Yun, T. Yun, P. Kim, K. E. Lee, W. J. Lee, R. Ryoo, D. J. Pine, G. R. Yi, S. O. Kim, *Nano Lett.* **2014**, *14,* 1388.
[36] M. M. Cui, T. Emrick, T. P. Russell, *Science* **2013**, *342,* 460.
[37] N. Bowden, F. Arias, T. Deng, G. M. Whitesides, *Langmuir* **2001**, *17,* 1757.
[38] W. Wang, S. Chang, A. Gizzatov, *ACS Appl. Mater. Inter.* **2017**, *9,* 29380.
[39] H. E. Ries, *Nature* **1979**, *281,* 287.
[40] L. D. Zarzar, V. Sresht, E. M. Sletten, J. A. Kalow, D. Blankschtein, T. M. Swager, *Nature* **2015**, *518,* 520.

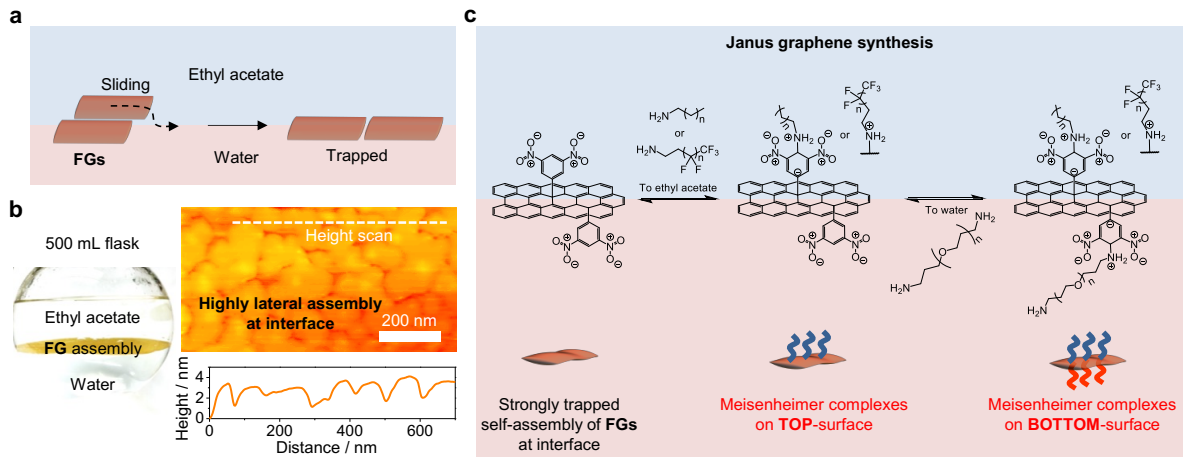

Figure 1. Self-assembly of FGs and JG synthesis at interface. (a) An assembly of individualized **FG** sheets forms at the ethyl acetate-water interface, as a result of the high density of 3,5-dinitrophenyl groups on the π-conjugated surfaces that significantly reduce interlayer stacking. (b) Left: A photograph of the large area **FG** assembly in a 500 mL flask. Right: atomic force microscopy (AFM) topology of the **FG** assembly that was lifted from the liquid interface onto a mica substrate. (c) Synthetic procedure for the preparation of 2-D **JG** using orthogonal Meisenheimer complex formation on interfacially trapped **FG** with 3,5-dinitrophenyl groups.

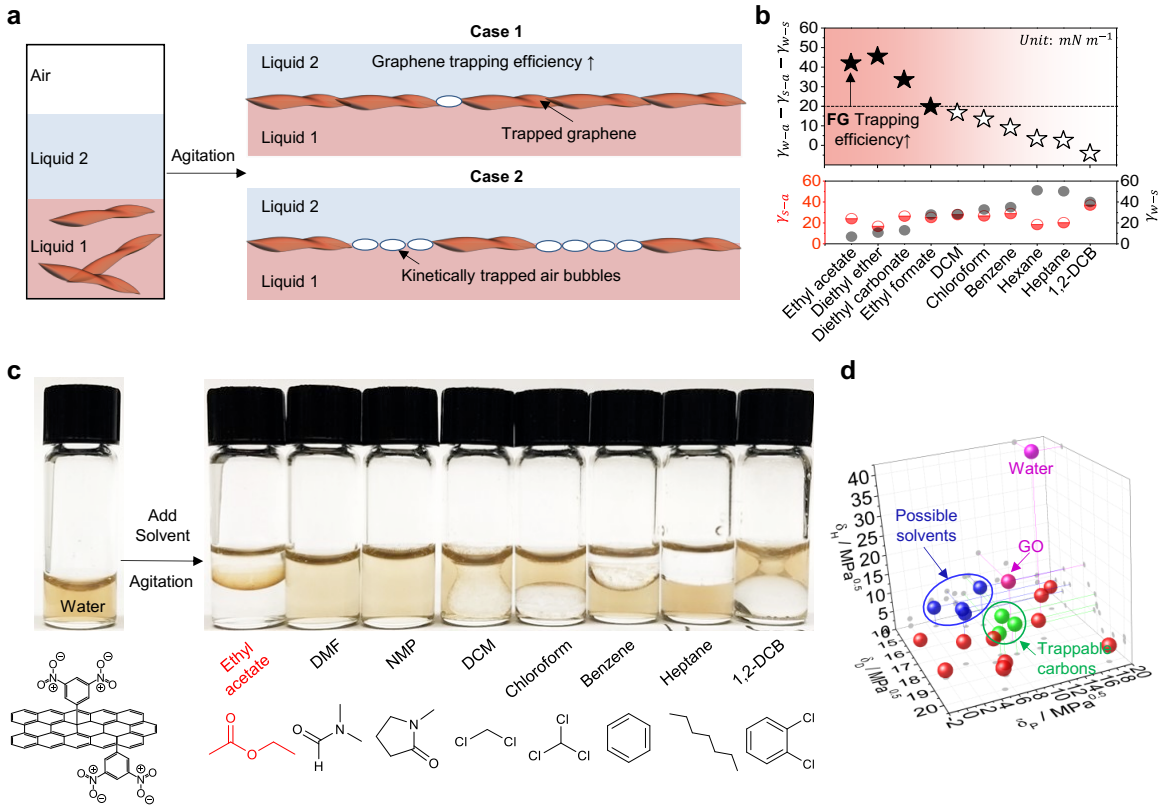

Figure 2. Interfacial trapping of FGs at the agitated liquid interface. (a) Graphenes assemble in an agitated immiscible Liquid−Liquid solution with interfacial trapping at the interface. In Case 1 with Liquid 1−Liquid 2, graphene is energetically driven to occupy effectively all of the liquid−liquid interface. For Case 2, it is energetically favorable for both graphene and air to occupy the interface of an immiscible Liquid 1−Liquid 2 interface. (b) Summary of the interfacial tensions of various liquid−air systems. (c) **FGs** are dispersed in the water phase and each solvent is added and then mixed. **FGs** assemble as a film only at the interface of ethyl acetate/water system. In the other cases, the **FG** persists in the water phase. (d) Hansen solubility parameters plot for solvents as a function of dispersive (δ_D), polar (δ_P), and hydrogen bonding (δ_H) interactions. Water-immiscible solvents within the blue circle cause **FGs** to localize at the interface. Green Dots represent: graphene, reduced graphene oxide (**rGO**), and unfunctionalized carbon nanotube (**CNT**). The high degree of oxygen functionality in **GO** results in strong H-bonding interactions with water, and trapped **GOs** are not observed at the interface.

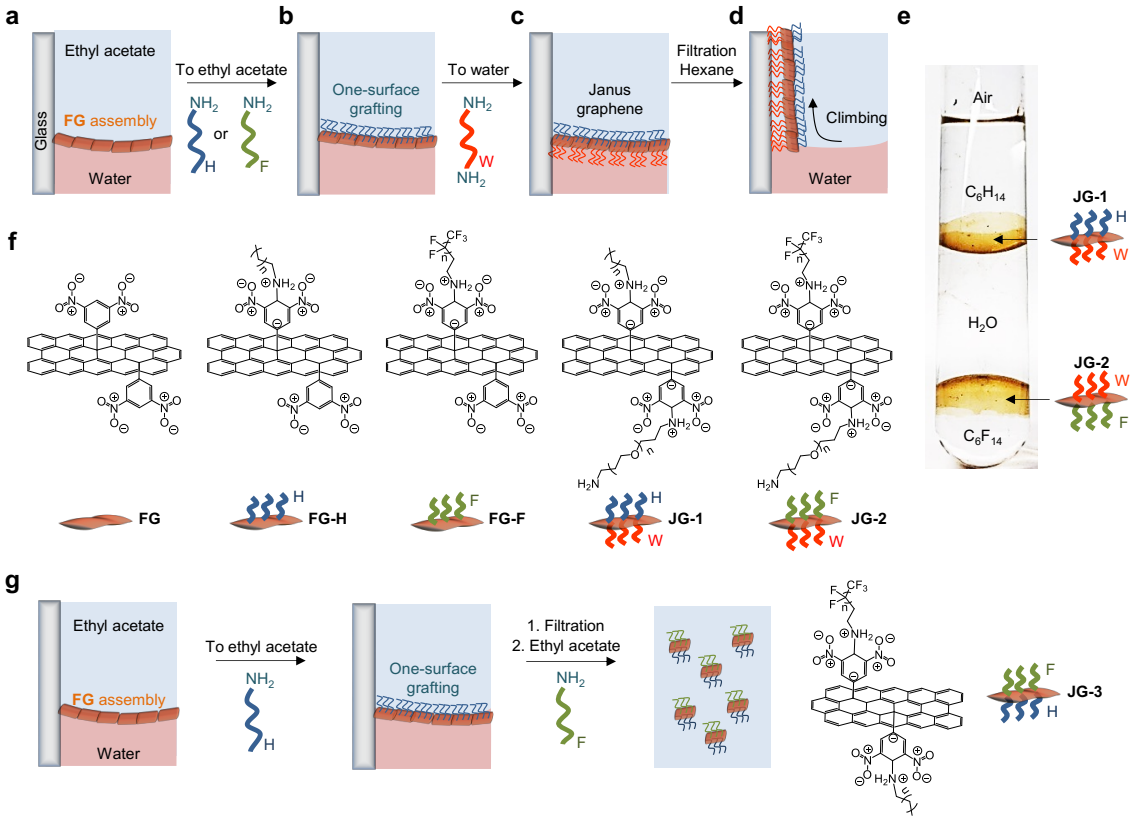

Figure 3. Schematic of the procedure to create FG-H, FG-F, JG-1, JG-2, and JG-3. (a) **FG** adsorbs at the interface of ethyl acetate and water. (b) Linear **H** or **F** chains functionalize the upper surface of the **FG** at the interface to create **FG-H** and **FG-F**, respectively. (c) **JG-1**, or **JG-2** are formed by the addition of linear water-soluble **W** chains to the water phase. The functional groups are bound by Meisenheimer complexes formation that occurs on each of the graphene surfaces. The graphenes have two different chemical functionalities and stabilize immiscible liquid−liquid interfaces with complementary character. (d) **JG-1** climbs the hydrophilic glass wall of vials in mixed ethyl acetate-hexane-water system. (e) **JG-1** and **JG-2** are trapped in the water−hexane and water−perfluorohexane interfaces, respectively. (f) Chemical structures of **FG**, **FG-H**, **FG-F**, **JG-1** and **JG-2**. (g) Schematic procedure for the creation of **JG-3** by first isolating **FG-H** and then functionalizing in ethyl acetate with **F** chains.

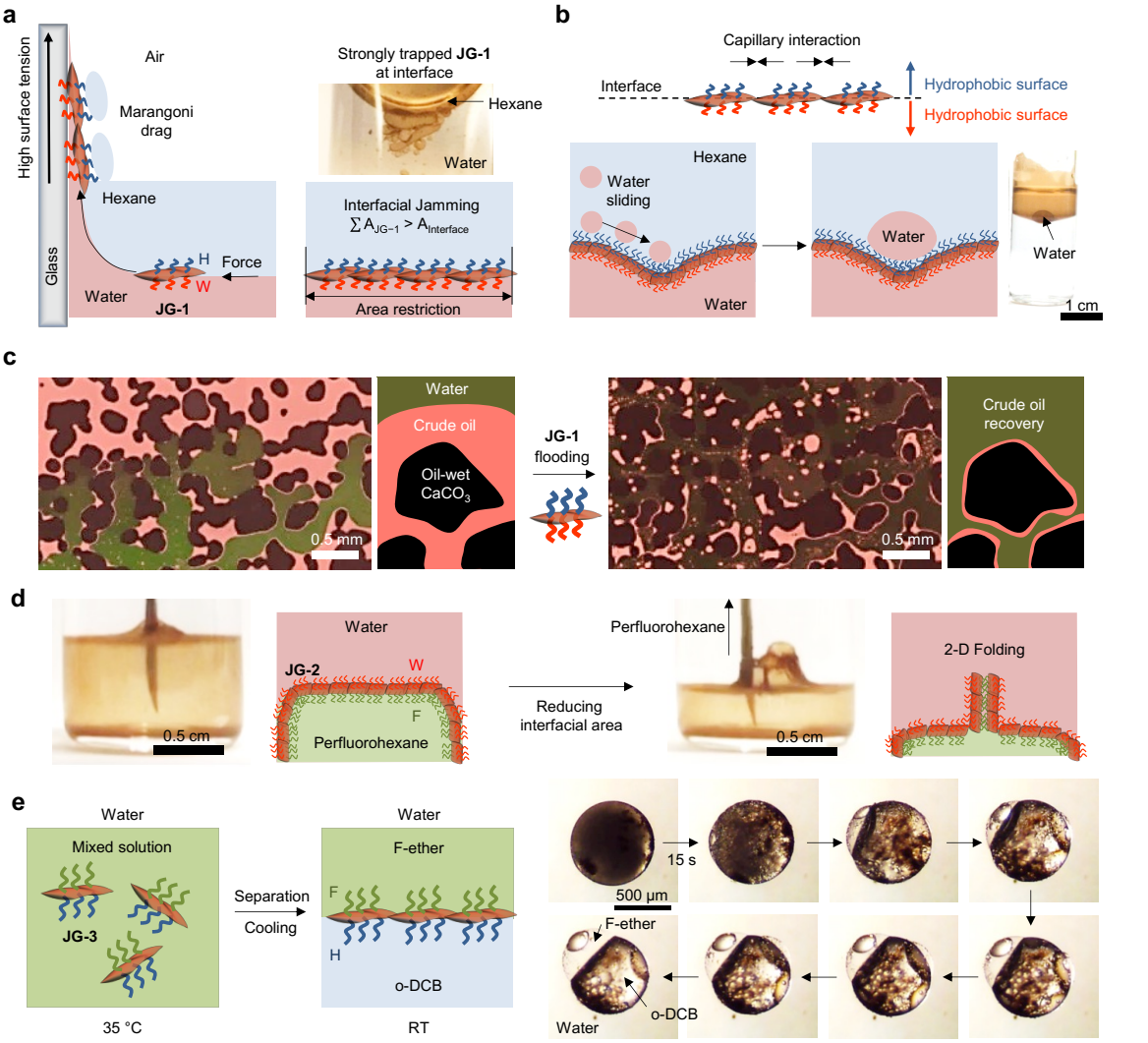

Figure 4. Applications of JGs. (a) (Left) **JG-1** climbs along the glass vial surface from the water–hexane interface to the air–glass interface with hexane through Marangoni flow. (Right) The interfacial jamming of the **JG-1** surfactants is observed. (b) The attractive capillary interactions are expected such that the structure is connected and forms a dense edge–edge assembly. Water droplets slide on the hydrophobic surface of the 2-D **JG-1** assembly. The assembly of **JG-1** at the interface supports a coalesced water droplet. (c) 2-D **JG-1** injection in the microfluidic system that emulates oil in a carbonate mineral formation. (Left) After water (green-dyed) flooding, 39 ± 2 % (determined by image processing) of crude oil (red) remained. (Right) After a **JG-1** water solution flooding, 25 ± 1 % of crude oil remained, indicating enhanced oil removal. (d) When the density of **JG-2** at the interface reaches the critical concentration, the **JG-2** experiences an attractive force and forms bi-layer assembly above the interface. (e) At elevated temperature 35 °C above Tc, *1,2*-DCB and F-ether with **JG-3** are miscible and emulsified in aqueous 0.1 % Zonyl FS-300 and 0.1 % sodium dodecyl sulfate. Below Tc, the mixed phase separates to create a Janus droplet in water. During cooling, **JG-3** moves to the *1,2*-DCB and F-ether interface.

We report a dynamic covalent assembly that directs graphene functionalization at liquid−liquid interfaces. This process imparts Janus characteristics to the graphene with different chemical functionality on its top and bottom faces. The dynamic covalent functionalization is accomplished via equilibrated Meisenheimer complexes produced by reactions of primary amines with pendant dinitroaromatics attached to the self-assembled graphenes.

Keyword: Janus, graphene, interfacial trapping, self-assembly, interfacial arrangement

Janus Graphene: Scalable Self-assembly and Solution-Phase Orthogonal Functionalization

Intak Jeon, Martin D. Peeks, Suchol Savagatrup, Lukas Zeininger, Sehoon Chang, Gawain Thomas, Wei Wang and Timothy M. Swager*

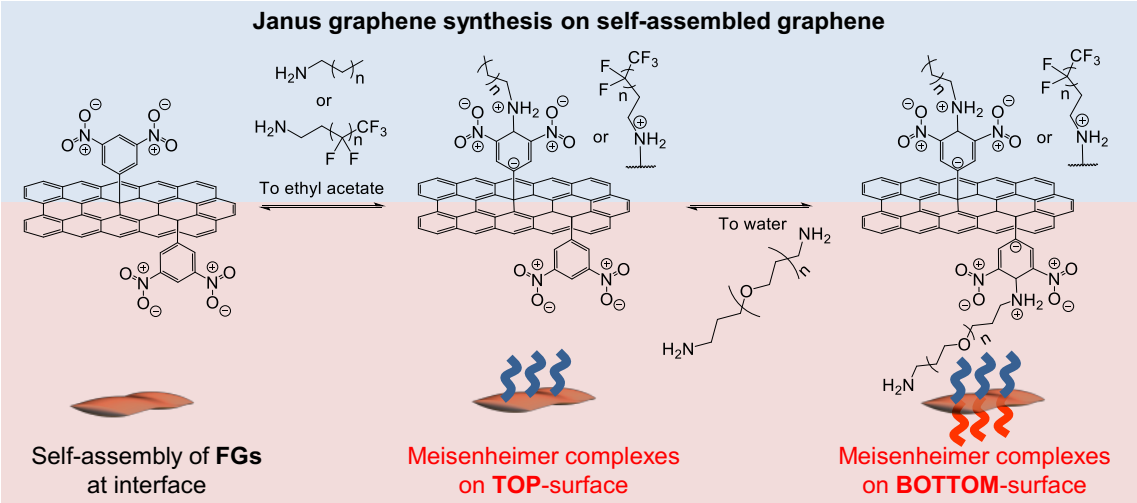

((Supporting Information can be included here using this template))

Supporting Information

Janus Graphene: Scalable Self-assembly and Solution-Phase Orthogonal Functionalization

Intak Jeon, Martin D. Peeks, Suchol Savagatrup, Lukas Zeininger, Sehoon Chang, Gawain Thomas, Wei Wang and Timothy M. Swager*

Movie 1. The dispersed **FG**s in water assemble at the interface of ethyl acetate−water during a brief period of agitation (real time).

Movie 2. High-speed optical video (frame rate: 1000 fps) for the interfacial trapping process of **FGs** in the interface of ethyl acetate−water in a quartz cuvette.

Movie 3. The assembly of **FG** with kinetically trapped air at the interface of ethyl acetate−water is forced to be rearranged by the diffusion (from top-phase ethyl acetate to the interface) of rhodamine B dye into the interface (real time).

Movie 4. High-speed optical video (frame rate: 240 fps) for the climbing process of **JG-1** in the water−hexane system in a vial.

Movie 5. When the assembly of **JG-2** at the interface of water−perfluorohexane reaches the critical concentration, the **JG-2** forms a bi-layer assembly above the interface. The volume of perfluorohexane is slowly using a syringe (real time).

Movie 6. The mixture of *1,2*-DCB and ethyl nonafluorobutyl ether with **JG-3** is emulsified in aqueous 0.1 % Zonyl FS-300 and 0.1 % sodium dodecyl sulfate. Cooling from elevated temperature (35 °C) to room temperature induces the phase separation of the *1,2*-DCB and ethyl nonafluorobutyl ether solvents. **JG-3** displays a complex interfacial rearrangement at the *1,2*-DCB and ethyl nonafluorobutyl ether interface (real time).

Methods

Chemicals. The following chemicals were used as received: highly oriented pyrolytic graphite (HOPG), tetrabutylammonium perchlorate (TBAP), sodium dodecyl sulphate (≥99 %), Sudan Red 7B (95 %), Rhodamine B dye (95 %), Zonyl FS-300 (40 % solids), hexadecafluorodecane (97 %), methoxyperfluorobutane (99 %), perfluorohexanes (98 %), ethyl nonafluorobutyl ether (>98 %), ethyl acetate, dimethylformamide (DMF), acetonitrile (MeCN), *N*-methyl-2-pyrrolidone (NMP), dichloromethane (DCM), chloroform, benzene, heptane, 1,2-dichlorobenzene (*1,2*-DCB), ethyl ether, benzyl benzoate, ethyl formate, propylene carboitjeonnate, diethyl carbonate, *n*-octylamine (**H**), 4,7,10-trioxa-1,13-tridecanediamine (**W**), and 1*H*,1*H*,2*H*,2*H*-perfluorooctylamine (**F**).

Synthesis of 3,5-dinitrophenyl functionalized graphene. We previously reported the electrochemical method of 3,5-dinitrophenyl functionalized graphenes from a Hyper-3-Stage-1 graphite intercalation compound (Ref. [20] in main text).

Interfacial trapping of graphenes. Interfacial trapping of graphenes was tested with ethyl acetate, DMF, MeCN, NMP, DCM, chloroform, benzene, heptane, *1,2*-DCB, ethyl ether, benzyl benzoate, ethyl formate, propylene carbonate, diethyl carbonate and methyl nonafluorobutyl ether, perfluorohexane, 3-ethoxyperfluoro(2-methylhexane), and ethyl perfluorobutyl ether. 3,5-dinitrophenyl functionalized graphene was added to a water-ethyl acetate solvent system (50:50 %, v/v) and then the liquid systems were agitated to generate short-lifetime emulsions. The total area of 3,5-dinitrophenyl functionalized graphenes is less than the area of the liquid−liquid interface. Ethyl acetate emulsion with 3,5-dinitrophenyl functionalized graphene immediately formed and then in a short period of time the graphenes were trapped at the interface. Graphene spontaneously assembles into a uniform film at the interface of water and ethyl acetate. This process proceeds with Rayleigh-Bénard convection and Marangoni forces at the interface, leading to a graphene assembly. Materials with low hydrogen bonding interactions with water, including graphene, **rGO** and **CNT**, are trappable at the interface. **FG** is expected to have the lower hydrogen boding parameter than **GO**.

Fabrication of Janus Graphenes (JGs). The water and ethyl acetate system have two distinct phases after shaking even though they are partially miscible. For more precise interfacial chemistry on **FGs** it is essential for the system to reach equilibrium before further functionalization. *n*-octylamine (100 μL) was introduced to ethyl acetate under mild stirring or no stirring. Interfacial trapped graphenes at the interface of water and ethyl acetate reacted with *n*-octylamine via the Meisenheimer complexation reaction, forming single-sided functionalized graphene with hydrocarbon alkyl chains. After the single-sided functionalization, 4,7,10-trioxa-1,13- tridecanediamine was introduced to water. Again, this amine reacts with 3,5-dinitrophenyl functionalized graphene, forming **JG-1** with hydrocarbon alkyl chains and water-soluble chains. Volatile ethyl acetate evaporated and the assembly of **JG-1** was transferred to other solvents for washing. The **JG-1s** were washed with ethyl acetate and acetone. **JG-2** and **JG-3** were fabricated in a similar manner.

Oil recovery system in microfluidic channel. Calcium carbonate ($CaCO_3$)–coated microfluidic chips were filled with crude oil and aged in a pressure-tight vessel at a high temperature (95 °C) for a month (Ref. [38] in main text). The oil-saturated chip was imaged using a Zeiss inverted optical microscope in epifluorescence mode. Automated tile scanning was used to image the entire microfluidic chip area. The crude oil was visible in epifluorescence due to its broadband fluorescence between 500-700 nm. After imaging the fully-saturated chip, deionized water with 10^{-4} M fluorescein was injected into the chip at

1 μL min^{-1}. Fluorescein has a strong emission peak at 512 nm making it visibly distinguishable from the crude oil fluorescence. Using a triplebandpass filter and Zeiss AxioCam HRc RGB camera, the fluorescein/water appears green while the crude oil appears red. Full-chip images were collected every hour during water flooding until a steady state was reached at which no additional oil flowed from the chip. After steady state, the **JG-1** (91 μg mL^{-1}) solution was injected at 1 μL min^{-1}. Additional images were collected every hour until the steady state was reached (12 hr). To quantify the amount of oil in the chip, each image was cropped to the chip area and ImageJ software was used to count the number of red pixels (using intensity threshold) relative to the total image size. The first image was used as a reference representing 100% oil saturation, and subsequent images were reported as a percentage of the full saturation. The incremental oil recovery is the difference between the percentage of oil remaining before and after **JG-1** injection.

Interfacial rearrangement of JG-3. Complex droplets of *1,2*-DCB and ethyl nonafluorobutyl ether were emulsified in the surfactant solutions comprising sodium dodecyl sulphate (SDS, an anionic hydrocarbon surfactant) and Zonyl FS-300 (Zonyl, fluorocarbon surfactant) at equal mass using methods described previously (Ref. [40] in main text). Briefly, the dispersion of **JG-3** in *1,2*-DCB and ethyl nonafluorobutyl ether were heated above the critical solution temperature. The heated mixture was then emulsified via either bulk emulsification or in a microfluidic device to yield polydisperse or monodisperse emulsions, respectively. Cooling to room temperature resulted in phase separation of the hydrocarbon and fluorocarbon solvents, yielding the complex emulsions with uniform composition of the two solvents in every droplet. To observe the interfacial rearrangement of **JG-3**, the complex droplets were re-heated above the critical temperature under an optical microscope and were allowed to slowly cool to room temperature.

Critical mixing temperature determination for JG-3. Polydisperse complex droplets comprising 1:1 mixture of the dispersion of **JG-3** in *1,2*-DCB and ethyl nonafluorobutyl ether were emulsified at elevated temperature and cooled down to room temperature. To obtain the precise critical temperature at which the hydrocarbon and fluorocarbon become miscible, controlled heating of the complex droplets was performed under an optical microscope. The stage was heated from 30 to 35 °C with an increment of 0.5 °C. At each temperature step, the droplets were allowed to equilibrate to the stage temperature for 3 minutes before the optical micrographs were captured. As a control, droplets without **JG-3** were subjected to the same treatment.

Characterization techniques. NMR spectra were measured on a Bruker Avance 400 spectrometer at 298 K. DOSY spectra were recorded using a linear gradient ramp of 16 steps, Δ = 70 ms, δ = 1250 μs, and around 100 scans. The LED experiment with bipolar gradients (ledbpgp2s) was employed. Data were worked up in TopSpin 3.5 pl7. Raman spectroscopy (Horiba HR800) with laser excitation wavelength of 532 nm was used to evaluate 3,5-dinitrophenyl functionalized graphene. The laser spot size is about 1 μm. X-ray photoelectron spectroscopy (XPS) measurements were carried out using a Physical Electronics Versaprobe II with Al Kα monochromatic X-ray at low pressures of below 2×10^{-8} Torr. Bright-field optical images were taken with a Zeiss Axiovert 200 inverted microscope equipped with a Zeiss AxioCam HRc camera.

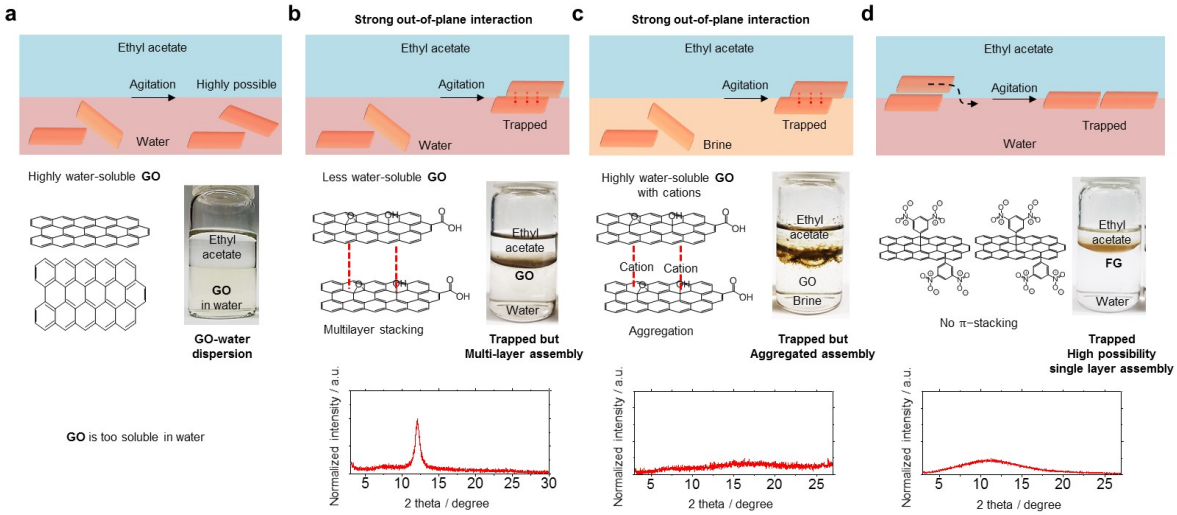

Figure S1. (a) Since **GO** is highly soluble in water, **GOs** remain in the water phase. (b) Although less water-soluble **GOs** are trapped at the water−ethyl acetate interface, the **GOs** are aggregated or form multi-layer assemblies at the interface through partial intersheet π−π stacking and hydrogen bonds. (c) When highly water-soluble **GOs** experience stronger attractions with cations, we can clearly see the aggregation at the interface. (d) The lateral assembly of **FGs** is efficiently trapped at the interface.

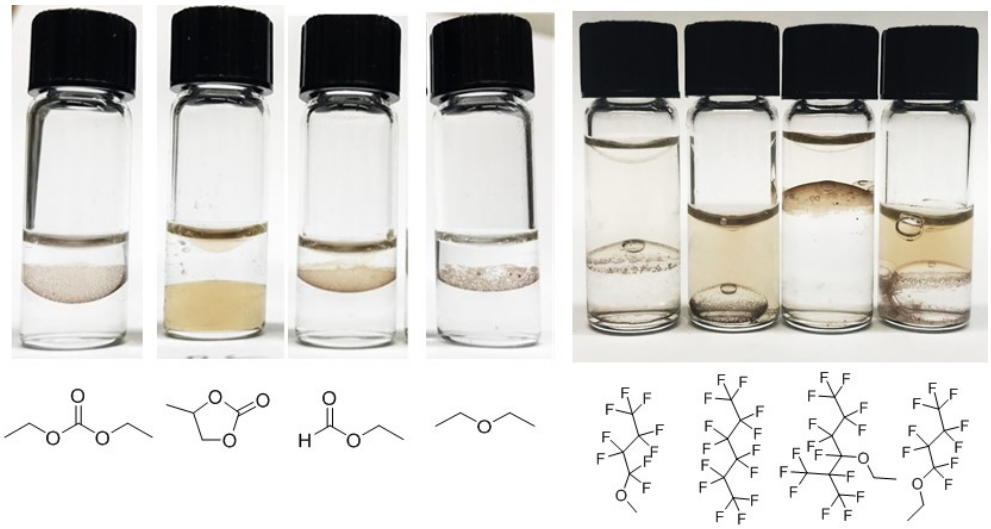

Figure S2. Interfacial trapping of **FGs** in various liquid systems with water. From left to right: diethyl carbonate, propylene carbonate, diethyl formate, diethyl ether, methyl nonafluorobutyl ether, perfluorohexane, 3-ethoxyperfluoro(2-methylhexane), and ethyl perfluorobutyl ether.

Solvent name	Dispersion, δ_D ($MPa^{0.5}$)	Polarity, δ_P ($MPa^{0.5}$)	Hydrogen bonding, δ_H ($MPa^{0.5}$)
Ethyl acetate	15.8	5.3	7.2
Dimethylformamide (DMF)	17.4	13.7	11.3
Heptane	15.3	0	0
Benzene	18.4	0	2.0
1,2-dichlorobenzene (o-DCB)	19.2	6.3	3.3
Diethyl ether	14.5	2.9	5.1
Methyl formate	15.3	8.4	10.2
N-methyl-2-pyrrolidone (NMP)	18	12.3	7.2
Water	15.6	16	42.3
Chloroform	17.8	3.1	5.7
Diethyl carbonate	15.1	6.3	3.5
Propylene carbonate (PC)	20	18	4.1
Benzyl benzoate (BB)	20	5.1	5.2
Dichloromethane (DCM)	18.2	6.3	6.1
Acetonitrile (MeCN)	15.3	18.0	6.1
Materials			
Graphene	18	9.3	7.7
Reduced graphene oxide (**rGO**)	17.9	7.9	10.1
Graphene oxide (**GO**)	17.1	10	15.7
Carbon nanotube (**CNT**)	17.8	7.5	5.6

Table S1. Hansen solubility parameters of solvents and materials (Ref. [32, 33] in Main text).

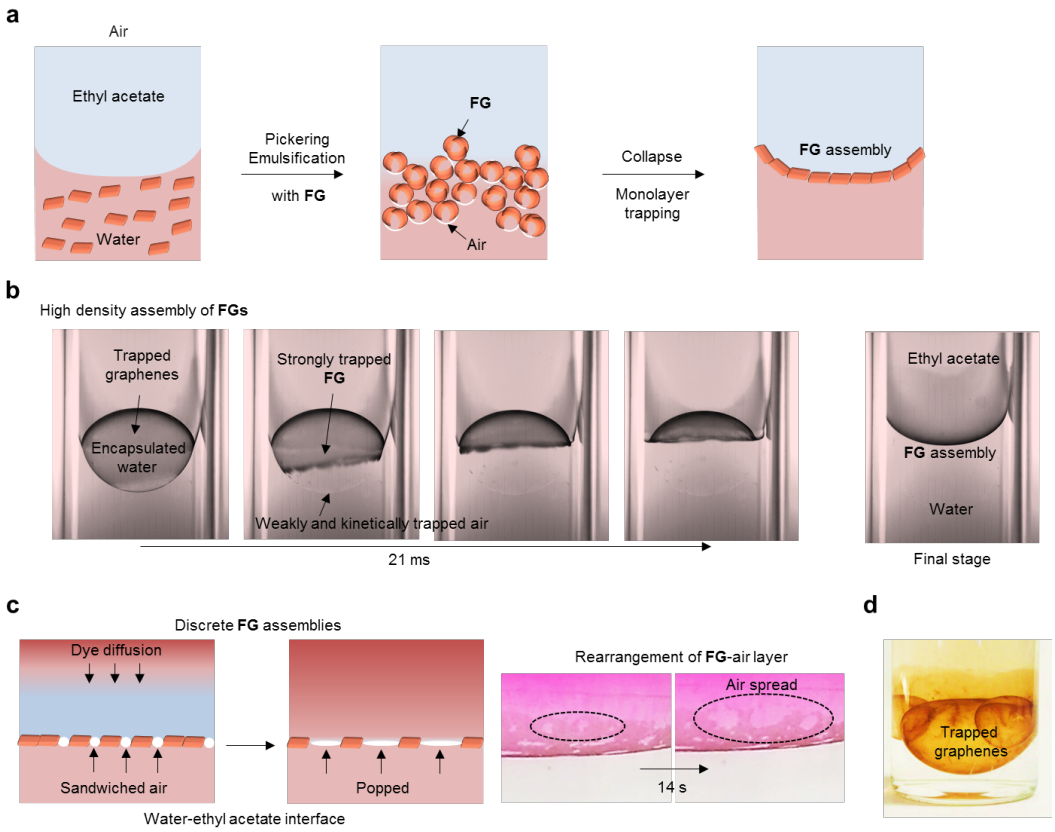

Figure S3. The assembly of FG and air at the interface. (a) Schematic illustration of interfacial trapping procedure of **FG** in water/ethyl acetate system. After mixing two immiscible liquids, transient emulsion droplets wrapped by **FG**s aggregate near the interface. The droplets collapse and **FG** occupies the resulting interface. The desorption energy of **FG** at the interface is higher than thermal energy at k_BT, and the **FG** is a Pickering agent stabilizing the interface. (b) High-speed optical images for the interfacial trapping process in a quartz cuvette (10 mm). The transition indicates that the transient emulsion contains water, trapped **FG**, and kinetically trapped air after agitation. At a transient stage, the **FG** and air encapsulate water at the interface. The air layer shown as a ghost image in the later photos taken over 21 ms dissipates (absorbs) into the solvents and the encapsulated water joins the bulk water phase. (c) In case of low-density **FG** at the interface, we postulate that the open area at the interface is temporarily occupied by air bubbles. The diffusion of rhodamine B dye generates a surface tension gradient at the interface which is partially occupied by air. The air rearranges **FG** at the interface. (d) Pickering emulsions of **FG**s at the interface.

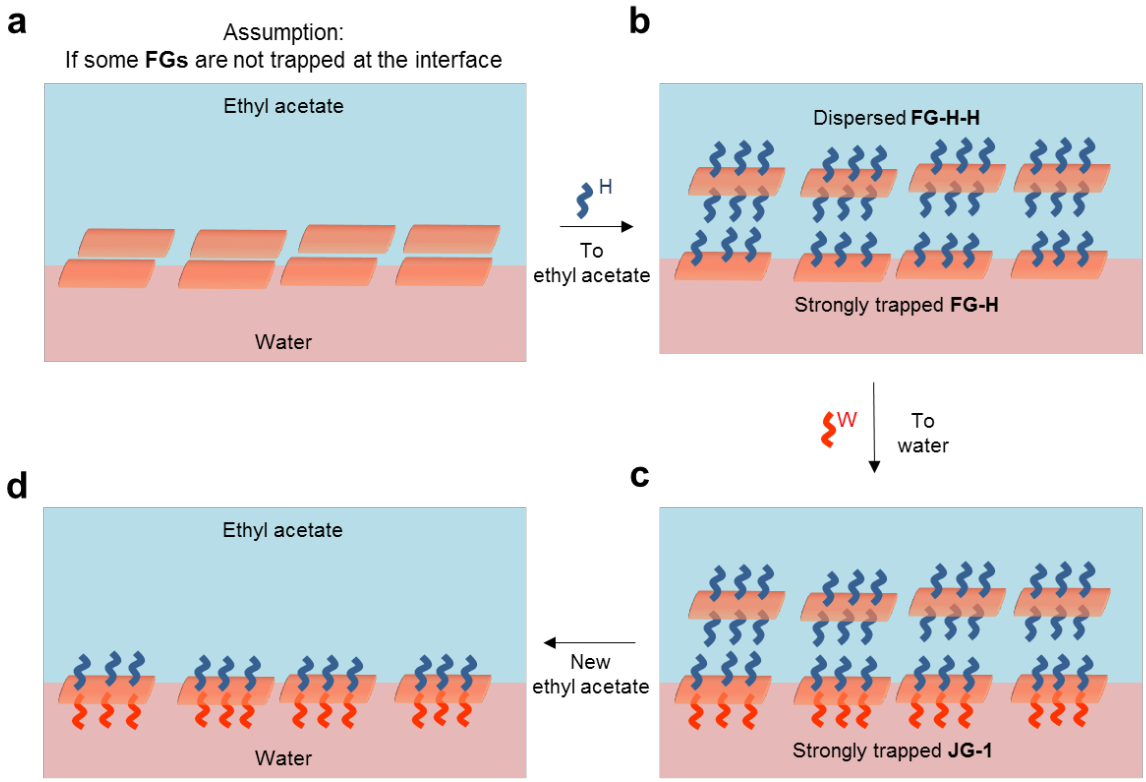

Figure S4. If some excess **FGs** are not trapped at the water−ethyl acetate interface, **FG-H-Hs** can be synthesized in ethyl acetate. The **FG-Hs**, however, are trapped at the interface so that the following Janus modification successfully completes at the interface. In this case, the **FG-H-Hs** are easily removed by replacing the ethyl acetate phase.

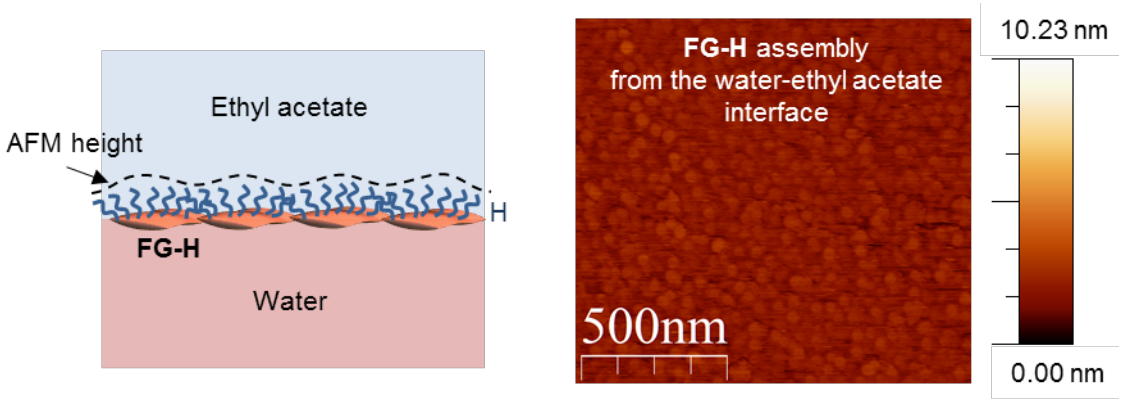

Figure S5. The atomic force microscopy (AFM) topology of the dense **FG-H** assembly, sampled from the interface of water and ethyl acetate, on a mica substrate.

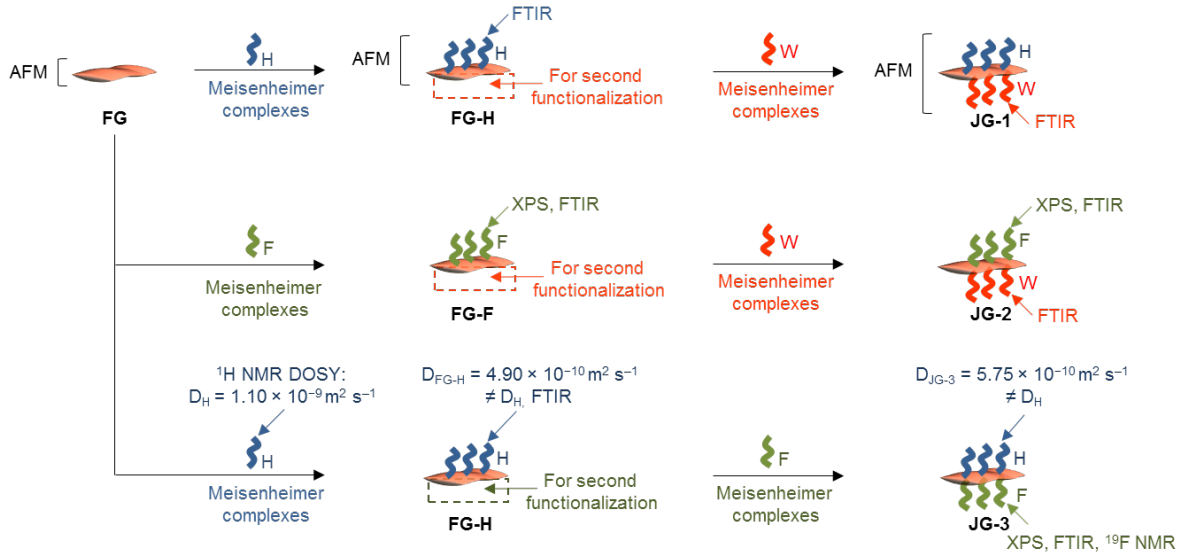

Figure S6. Orthogonally functionalized Janus graphene structure. The flowchart for the identification of chemical structures: **JG-1**, **JG-2**, and **JG-3**. The Meisenheimer complex **JGs** can be distinguishable by AFM, X-ray photoelectron spectroscopy (XPS), attenuated total reflectance–Fourier transform infrared spectroscopy (FTIR), and diffusion-ordered NMR spectroscopy (NMR ^{1}H DOSY) analyses. NMR ^{1}H-DOSY, are carried out in DMF-d_7 solution containing the graphenes. This provides distinguishable diffusion coefficients, D, as a function of the chemical shifts of the resonances associated with the graphenes: **H**, **FG-H** and **JG-3**.

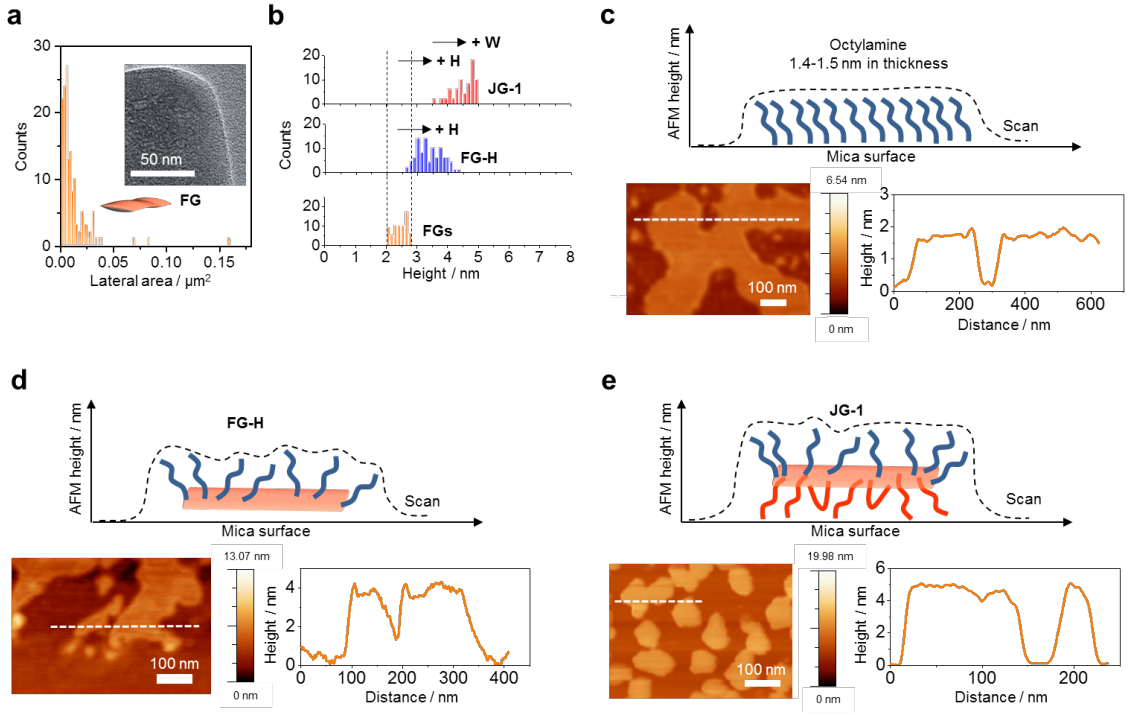

Figure S7. (a) The lateral size distribution of **FG**, sampled by transmission electron microscopy (TEM). (b) The thickness distribution of **FG**, **FG-H**, and **JG-1**, sampled by AFM. Representative AFM topology of (c) *n*-octylamine (**H** combination) (d) **FG-H**, and (e) **JG-1**.

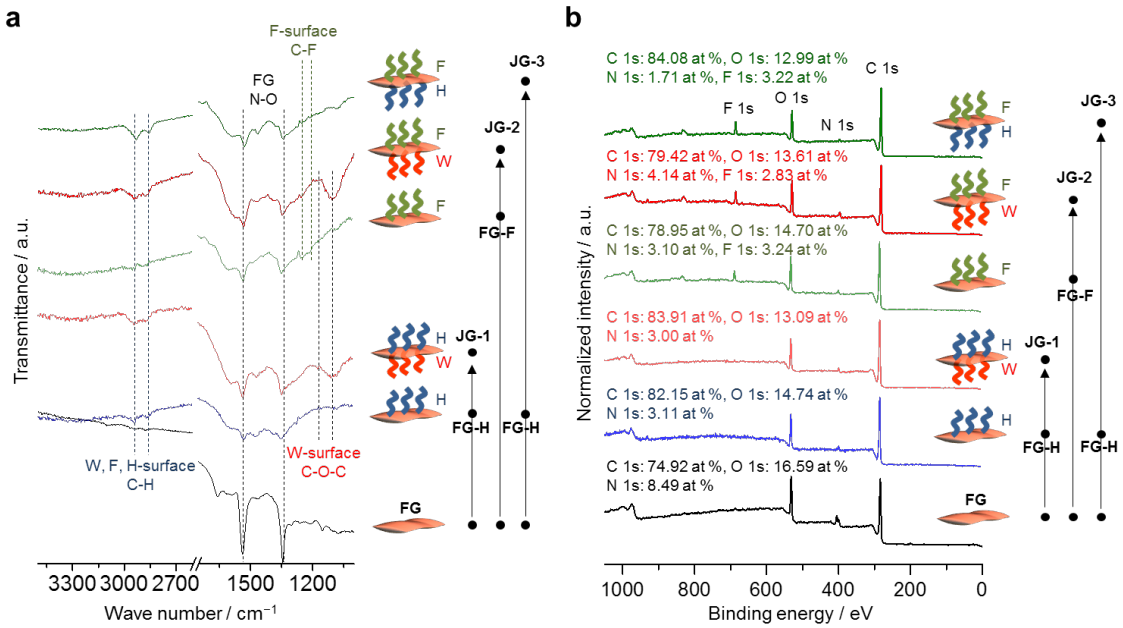

Figure S8. (a) Attenuated total reflectance-Fourier transform infrared (ATR-FTIR) and (b) X-ray photoelectron spectroscopy (XPS) spectra of (Bottom to Top) **FG**, **FG-H**, **JG-1**, **FG-F**, **JG-2**, and **JG-3**. ATR-FTIR and XPS spectra confirm that the *n*-octylamine, water-soluble 4,7,10-trioxa-1,13-tridecanediamine, or *1H,1H,2H,2H*-perfluorodecylamine were co-grafted successfully. When **JGs** form, the asymmetric stretch υ(N-O) shifts from 1538.9 cm^{-1} on **FG** to 1526.9, 1531.2, 1529.8, 1533.2, and 1529.7 cm^{-1} on **FG-H**, **JG-1**, **FG-F**, **JG-2**, and **JG-3**, respectively. The FTIR spectra show υ(C-H) in **FG-H**, **JG-1**, **JG-2**, and **JG-3**, and υ(C-O-C) in **JG-1**, and **JG-2**. In addition, the XPS survey spectra reveal clear F 1s peaks in **FG-F**, **JG-2**, and **JG-3**.

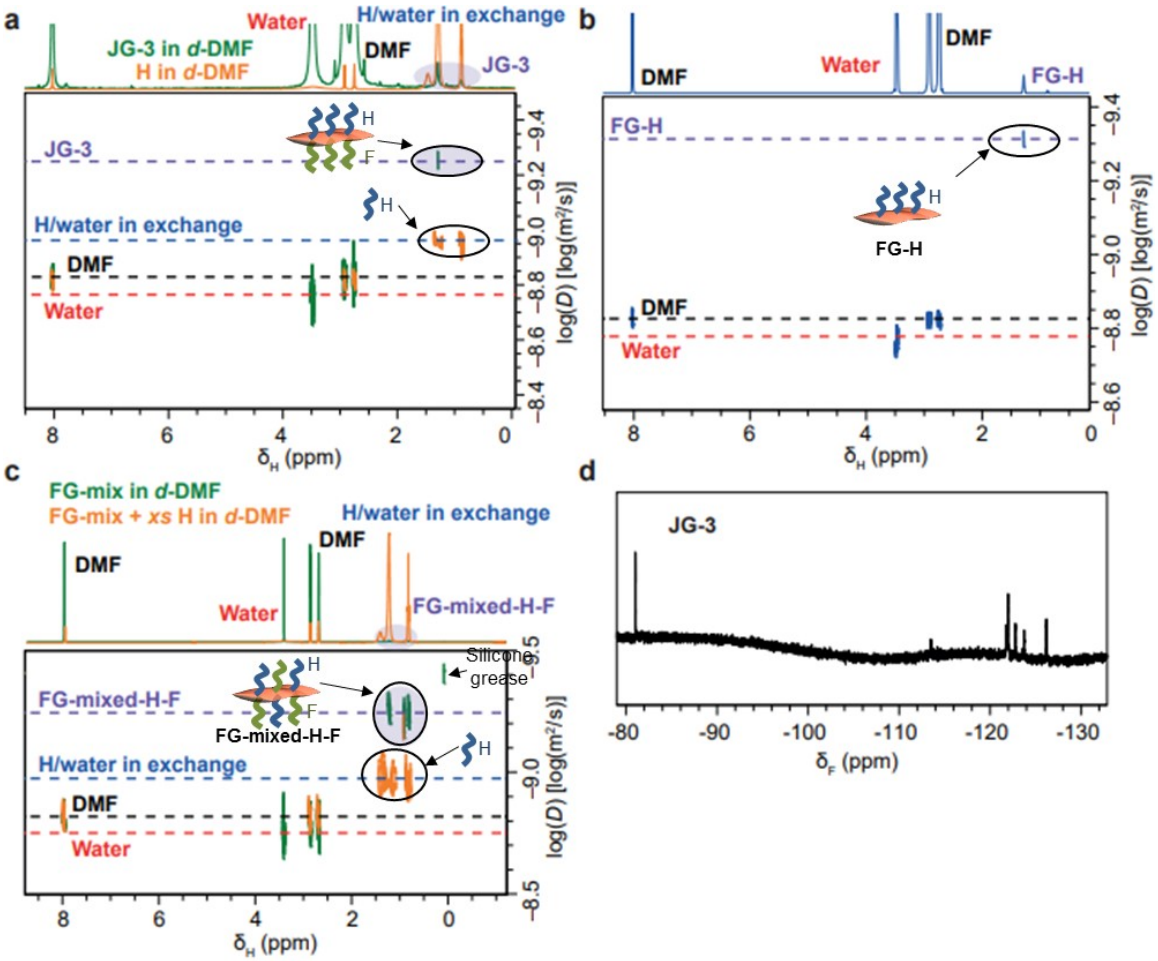

Figure S9. NMR ^{1}H-DOSY spectra of (a) **JG-3**, or **H**, (b) **FG-H**, and (c) **FG-mixed-HF**, or **H** ($D_{\mathbf{FG\text{-}mixed\text{-}H\text{-}F}} = 5.37 \times 10^{-10}$ m^2 s^{-1}). The ^{1}H DOSY spectra of **FG-H** ($D_{\mathbf{FG\text{-}H}} = 4.90 \times 10^{-10}$ m^2 s^{-1}) and **JG-3** ($D_{\mathbf{JG\text{-}3}} = 5.75 \times 10^{-10}$ m^2 s^{-1}) were measured to confirm that the observed aliphatic resonances (0.5 – 1.5 ppm) did not arise from residual **H** ($D_{\mathrm{H}} = 1.10 \times 10^{-9}$ m^2 s^{-1}). In case of **JG-3**, the remarkable change in diffusion coefficients provides clear and convincing evidence for the successful Meisenheimer complexes formation on **FGs**, where the chemical surfaces are functionalized with amines. Note that the rest of 3,5-dinitrophenyl groups on the opposite surface of **FG-Hs** allows the formation of asymmetrical Janus structures. (d) ^{19}F NMR of **JG-3** (298 K, 565 MHz, *d*-DMF). The successful incorporation of the fluorous chain in **JG-3** is confirmed by the presence of resonances in the ^{19}F NMR. These ^{19}F resonances are absent in **FG-H**.

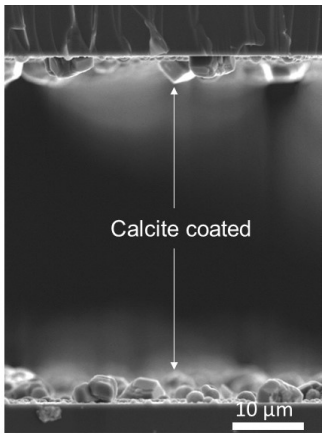

Figure S10. A cross-section scanning electron microscope (SEM) image of calcite coated microfluidic chip.

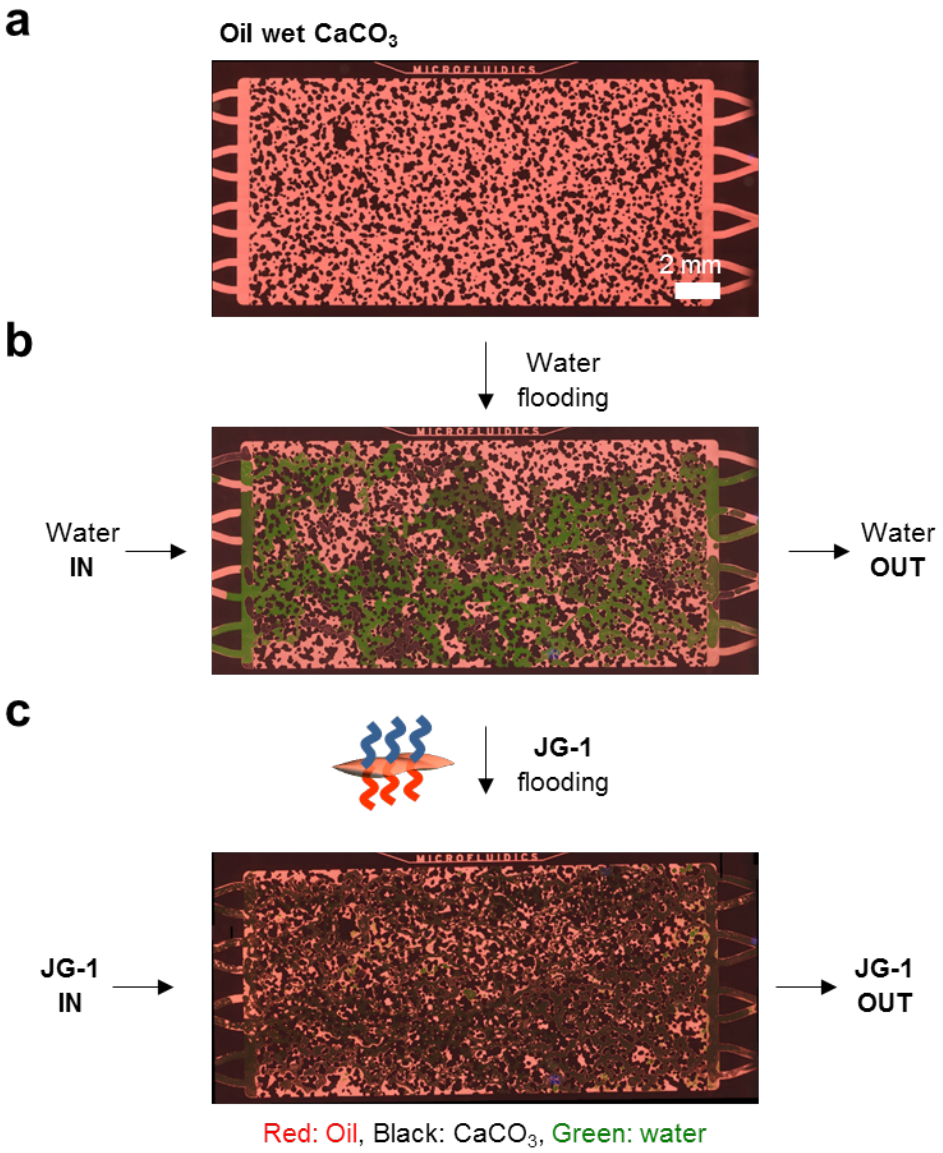

Figure S11. The calcium carbonate ($CaCO_3$) micromodel was prepared by growing a thin layer of $CaCO_3$ nanocrystals *in situ* in microfluidic channels to simulate carbonate reservoirs (total pore volume: 2.4 µL). Fluorescence images of a microfluidics chip with filled crude oil shows the oil recovery process in the calcite-coated reservoir chip obtained after (a) initial crude oil saturation, (b) water flooding, and (c) water with **JG-s** flooding by a widefield optical fluorescence microscope (see also **Figure 4c** in main text)

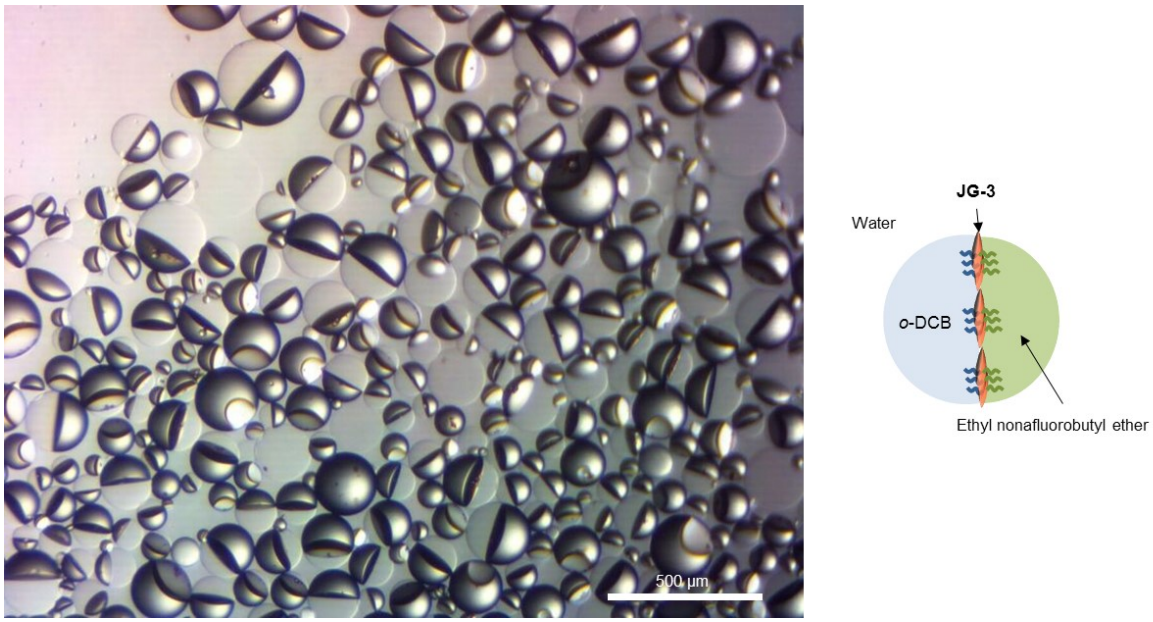

Figure S12. Optical micrograph and illustration of *1,2*-dichlorobenzene (*1,2*-DCB) and ethyl nonafluorobutyl ether Janus droplets with **JG-3s** trapped at the interface in water.

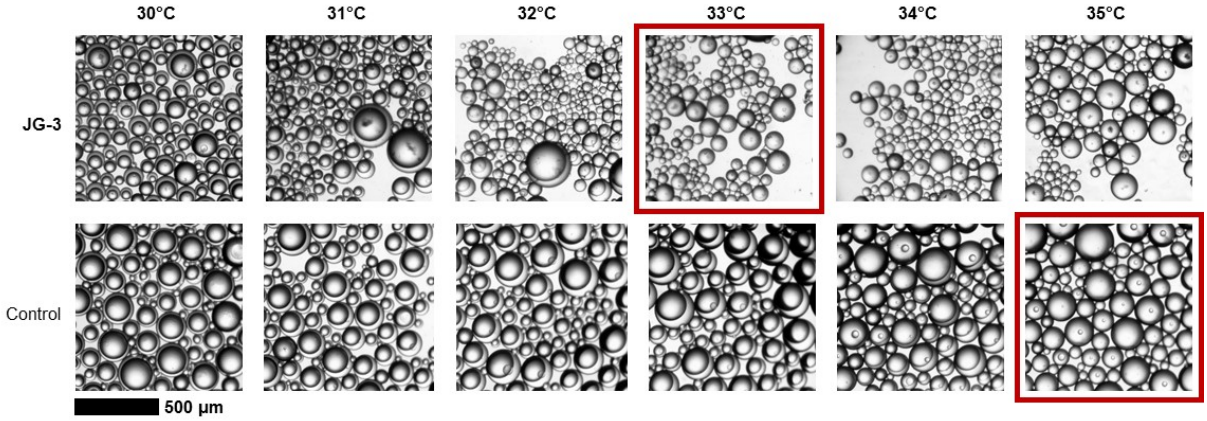

Figure S13. Droplets containing **JG-3** showed a lower mixing temperature of 33 ºC when compared to those without at 35 ºC. Each set of droplets were cycled between 30 and 35 ºC for 3 cycles; the mixing temperature were found to be within 0.5 ºC (or the resolution of the experiment). The lower mixing temperature afforded by the inclusion of **JG-3** hinted at the lower interfacial tension between the hydrocarbon and fluorocarbon phases, suggesting that **JG-3** has an impact on the interface of the two phases.